Polarization Diversity Pulse-Pair Technique for Millimeter-Wave Doppler Radar Measurements of Severe Storm Features

ANDREW L. PAZMANY AND JOHN C. GALLOWAY

Microwave Remote Sensing Laboratory, University of Massachusetts, Amherst, Amherst, Massachusetts

JAMES B. MEAD AND IVAN POPSTEFANIJA

Quadrant Engineering Inc., Amherst, Massachusetts

ROBERT E. MCINTOSH*

Microwave Remote Sensing Laboratory, University of Massachusetts, Amherst, Amherst, Massachusetts

HOWARD W. BLUESTEIN

School of Meteorology, University of Oklahoma, Norman, Oklahoma

(Manuscript received 6 October 1998, in final form 26 January 1999)

ABSTRACT

The Polarization Diversity Pulse-Pair (PDPP) technique can extend simultaneously the maximum unambiguous range and the maximum unambiguous velocity of a Doppler weather radar. This technique has been applied using a high-resolution 95-GHz radar to study the reflectivity and velocity structure in severe thunderstorms. This paper documents the technique, presents an analysis of the first two moments of the estimated mean velocity, and provides a comparison of the results with experimental data, including PDPP images of high-vorticity regions in supercell storms.

1. Introduction

The maximum unambiguous range r_{max} and maximum unambiguous velocity u_{max} of a conventional pulsed Doppler radar are related by (Doviak and Zrnić 1984; Miller and Rochwarger 1972)

$$r_{max}|u_{max}| = c\lambda/8, \quad (1)$$

where c is the speed of light and λ is the radar wavelength. While this ambiguity relation applies to all weather radars, millimeter-wavelength radars face a particularly stringent limit due to the increase in Doppler frequency shift with increasing operating frequency. This high Doppler shift often forces the operation of millimeter-wave radars to sacrifice range and accept multiple folding in the velocity data, even for moderate winds. For example, at 3 mm (95 GHz) wavelength the product of the maximum velocity and range is so small that for a u_{max} of ± 8 m s^{-1}, r_{max} is reduced to 14 km. These limitations may be acceptable during zenith observations of some clouds and precipitation; longer-range capability is often necessary during horizontal measurements, however, and weather phenomena such as convective clouds and storms require the ability to measure much higher wind speeds.

Conventional estimators of Doppler velocity, such as the Fourier transform and pulse-pair techniques, can measure beyond u_{max} by using multiple (staggered) pulse-repetition frequencies (PRF) (Doviak and Zrnić 1984); however, the performance of these estimators degrades when the standard deviation of the Doppler spectrum is large compared to the folding velocity. An increase in PRF increases the folding velocity but also decreases the maximum range, which can make interference from scatterers located past r_{max} more likely. Golestani et al. (1995) successfully reduced this interference by combining multiple polarizations with staggered PRFs, but this method did not remove the limitation imposed by (1).

Doviak and Sirmans (1973) proposed a polarization

* Deceased.

Corresponding author address: Dr. Andrew Pazmany, Microwave Remote Sensing Laboratory, University of Massachusetts, Amherst, Knowles Bldg., Amherst, MA 01002.
E-mail: pazmany@mirsl.ecs.umass.edu.

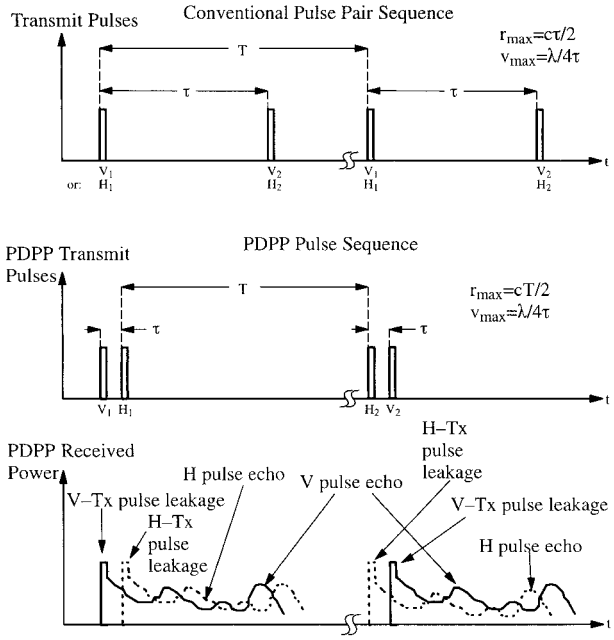

FIG. 1. Comparison of conventional pulse-pair sequence with polarization diversity pulse-pair sequence (PDPP).

diversity pulse-pair (PDPP) technique that can decouple r_{max} from u_{max}. The technique takes advantage of 1) the isolation between orthogonally polarized signals to prevent ambiguity and 2) the high degree of correlation between the orthogonal copolarized backscatter coefficients (S_{vv} and S_{hh}) of atmospheric particles to measure velocity. Figure 1 compares a conventional pulse-pair transmit polarization sequence with the PDPP sequence proposed by Doviak and Sirmans. The technique allows a radar system to measure the first two moments of the Doppler spectrum by simultaneously using two receiver channels to receive the scattered field from two closely spaced, orthogonally polarized pulses. The received signal from the two pulses then is processed like conventional pulse-pair signals. The resulting u_{max} measurement is limited only by the receiver bandwidth, and r_{max} has no theoretical limit because the pairs can be spaced as far apart as desired. In practice, however, operating with an excessively high u_{max} will unnecessarily increase the standard deviation of the Doppler measurements (as shown in section 3), and a very long r_{max} implies operation at low average power, which degrades sensitivity.

To the best of our knowledge, PDPP has not been implemented with a weather radar until this project, in spite of the potential benefit of the technique. There are two possible reasons for this. First, PDPP requires a complex radar system with two receiver channels that can simultaneously measure the orthogonal polarization components of the received electric field and can switch the transmit polarization from pulse to pulse. Second, complex, high-frequency weather radars with these capabilities only recently have been developed and low-frequency (S, C, X band) radars almost always can eliminate problems associated with the coupling of r_{max} with u_{max} using conventional staggered PRF techniques.

The PDPP technique was applied using the University of Massachusetts (UMass) 95-GHz polarimetric cloud radar (Pazmany et al. 1994a, 1994b; Bluestein et al. 1997) to the study of tornadoes and of substructures in supercell storms as part of a joint UMass and University of Oklahoma (OU) experiment. The PDPP technique is necessary because the combination of high operating frequency of the radar, the extreme wind speeds inside a tornado, and the difficulty and risks associated with getting close to a tornado requires high values of both r_{max} and u_{max}.

In the next section, the conventional pulse-pair technique and PDPP estimation of the first two moments of the reflectivity-weighted Doppler spectrum are described. In section 3, an expression for the standard deviation of the PDPP mean velocity estimate is derived and is compared to that of conventional pulse pair. In section 4, an interleaved PDPP and conventional pulse-pair sequence is described that minimizes Doppler measurement errors while extending both u_{max} and r_{max}. Images of the reflectivity and Doppler velocity of a severe storm that contained a cyclonic and an anticyclonic hook also are presented. Furthermore, section 4 presents comparisons of the conventional pulse-pair velocity images with the PDPP images and the standard deviation of the PDPP velocity measurements with the standard deviation predicted by the expression derived in section 3. The paper is concluded in section 5.

2. Pulse-pair techniques

The conventional pulse-pair technique estimates the first two moments of the reflectivity-weighted Doppler spectrum from the autocorrelation function of the radar signal at both zero lag and some lag τ. Since a Gaussian-shaped power spectrum is a good approximation of the Doppler spectrum of various turbulent media, the autocorrelation function may be expressed as (Zrnić 1977)

$$R(\tau) = R(0)\beta e^{j2\pi f_o \tau}, \tag{2}$$

where $R(0)$ is the signal power, f_o is the mean Doppler shift, and β is the normalized signal correlation. Here β is a function of the power spectrum standard deviation σ_f and the pulse-pair spacing τ according to

$$\beta = e^{-2\pi^2\sigma_f^2\tau^2}. \tag{3}$$

For $\tau \ll 1/\sigma_f$, the Doppler velocity mean and standard deviation can be approximated by (Doviak and Zrnić 1984; Miller and Rochwarger 1972)

$$\hat{\mu}_u = \frac{\lambda}{4\pi\tau} \arctan\left\{\frac{\mathcal{I}[R(\tau)]}{\mathcal{R}[R(\tau)]}\right\}, \quad (4)$$

and

$$\hat{\sigma}_u = \frac{\lambda}{2\sqrt{2}\pi\tau}\sqrt{1 - \frac{R(\tau)}{R(0)}}, \quad (5)$$

where $\hat{\mu}_u$ is the mean velocity estimate, $\hat{\sigma}_u$ is the spectral width estimate, and $\mathcal{R}$ and $\mathcal{I}$ represent real and imaginary components.

Spectral moment estimation from PDPP measurements takes a similar form; however, the autocorrelation function is replaced by the cross-correlation function of the orthogonally polarized signals. Again assuming Gaussian-shaped power spectra, and using a vertical (v) and horizontal (h) polarization basis, the cross-correlation function of the scattered field for a v–h pair R_{vh} can be expressed as

$$R_{vh}(\tau) = |R_{vh}(0)|\beta e^{j(2\pi f_o \tau + \phi)}. \quad (6)$$

Similarly, for an h–v pair, R_{hv} can be expressed as

$$R_{hv}(\tau) = |R_{hv}(0)|\beta e^{j(2\pi f_o \tau - \phi)}, \quad (7)$$

where the phase bias ϕ accounts for differential phase shift during propagation between the radar and the scatterers and for any difference in the transmission line lengths between the two polarization channels in the radar. Since this bias has an opposite sign when the polarization sequence is reversed, it can be eliminated by interleaving v–h pulse pairs with h–v pairs. After combining $R_{hv}(\tau)$ with $R_{hv}(\tau)$, the unbiased estimate of the mean velocity can be expressed as

$$\hat{\mu}_u = \frac{\lambda}{4\pi\tau} \arctan\left\{\frac{\mathcal{I}[\sqrt{R_{vh}(\tau)R_{hv}(\tau)}]}{\mathcal{R}[\sqrt{R_{vh}(\tau)R_{hv}(\tau)}]}\right\}. \quad (8)$$

The estimate of the standard deviation of the Doppler spectrum, similar to (5), can be expressed as

$$\hat{\sigma}_u = \frac{\lambda}{2\sqrt{2}\pi\tau}\sqrt{1 - \frac{|R_{vh}(\tau)|}{|R_{vh}(0)|}}; \quad (9)$$

$|R_{vh}(\tau)| = |R_{hv}(\tau)|$ is assumed. The practical use of (9) is limited, however, because $|R_{vh}(0)|$ is difficult to measure, especially in conditions when conventional pulse-pair technique breaks down. A technique outlined by Doviak and Zrnić (1984) for the estimation of $|R_{vh}(0)|$, for example, requires the measurement of the lag 2 autocorrelation $R_{hh}(2\tau)$. However, when this function can be measured, PDPP technique is not needed. The technique by Doviak and Zrnić (1984) could be modified to replace $|R_{hh}(2\tau)|$ with $|R_{vh}(2\tau)|$, which can be obtained from lag 2 PDPP measurements, but an a priori model for the power spectrum shape also is needed, which model is difficult to estimate in high-shear regions such as a tornado. Noncoherent polarimetric measurement technique (Mead et al. 1993; Pazmany and McIntosh 1994) may be used to estimate $|R_{vh}(0)|$, but this technique requires a complex radar that can transmit three or more linearly independent polarizations and can measure the polarization of the scattered field. Without this capability, $|R_{vh}(0)|$ may be approximated from the copolarized received power at vertical and horizontal polarizations and by assuming that S_{vv} and S_{hh} are completely correlated. This approximation, however, leads to an imprecise estimate of σ_u; therefore, it is useful only to locate regions that have very high spectral width, such as tornadoes.

The implementation of PDPP requires a polarimetric Doppler radar system with some unique capabilities. As seen in Fig. 1, the close pulse spacing and varying transmit polarization during PDPP measurements require a radar with fast transmit/receive and polarization switches, and the radar must have two receivers to measure simultaneously the scattering from the two orthogonally polarized transmit pulses. Such a radar system is the UMass W-band cloud radar, documented in Pazmany et al. (1994a), which was constructed with two receiver channels to speed the measurement of the polarimetric scattering properties of clouds and precipitation from an aircraft.

3. Polarization diversity pulse-pair estimate errors

The PDPP technique provides an unbiased estimate of the Doppler velocity and can be used to measure very high wind speeds effectively in the presence of high shear, but it sacrifices accuracy to achieve this. The high unambiguous velocity of PDPP is one of the main contributors to the relatively high estimate error because, with increasing $u_{\max}$, the error in the measured phase of the correlation function maps into a larger velocity error. These errors in the measured phase are generated by thermal and phase noise and by interference between the orthogonally polarized signals resulting from the finite polarization isolation of the antenna and orthomode transducer (OMT). These interfering ''noiselike'' signals add to thermal noise to decrease the effective signal-to-noise ratio, and therefore must be considered when estimating the standard deviation of PDPP velocity estimates. This analysis is presented next.

For a polarimetric radar, the measured voltage $\mathbf{V}_m$ that corresponds to scattering from range r at time t can be written in terms of the signal and noise components according to

$$\mathbf{V}_m(r, t) = \begin{bmatrix} V_{vv}(r, t) & V_{vh}(r, t) \\ V_{hv}(r, t) & V_{hh}(r, t) \end{bmatrix} + \begin{bmatrix} N_v(t) & N_v(t) \\ N_h(t) & N_h(t) \end{bmatrix}, \quad (10)$$

where V_{ij} is the signal component of the voltage at the output of the i-polarized receiver when j polarization was transmitted, and N_v and N_h represent system noise in the vertical and horizontal receiver channels, respectively. The signal component is a function of the target scattering matrix and matrices that characterize the po-

larimetric transformation of the signal during propagation according to Wood (1986)

$$\begin{bmatrix} V_{vv}(r,t) & V_{vh}(r,t) \\ V_{hv}(r,t) & V_{hh}(r,t) \end{bmatrix} = \frac{k}{r^2}\mathbf{D}_R\mathbf{D}_P\mathbf{S}[r, t-(r/c)]\mathbf{D}_P\mathbf{D}_T, \quad (11)$$

where $\mathbf{D}_R$ is the normalized [$\mathbf{D}_R(1, 1) = 1$] complex receiver distortion matrix, $\mathbf{D}_P$ is the normalized propagation distortion matrix that accounts for differential attenuation a and phase shift ϕ_p according to

$$\mathbf{D}_P = \begin{bmatrix} 1 & 0 \\ 0 & ae^{\phi_p} \end{bmatrix}, \quad (12)$$

$\mathbf{D}_T$ is the normalized complex transmitter distortion matrix, $\mathbf{S}(r, t)$ is the complex scattering matrix corresponding to the range cell located at a distance r from the radar at time t, and the complex constant k accounts for system gain and propagation effects. The estimate of the cross-correlation function $\hat{R}$ of the vertical and horizontal signals from M independent, closely spaced (small τ relative to the decorrelation time of the scattered signal) v–h pairs can be expressed as

$$\hat{R}_{vh}(r,\tau) = \frac{1}{M}\sum_{i=1}^{M}\{[V_{vv}(r,t_i) + V_{vh}(r-\Delta r, t_i) + N_v(t_i)] \times [V_{hh}(r, t_i+\tau) + V_{hv}(r+\Delta r, t_i+\tau) + N_h(t_i+\tau)]^*\}, \quad (13)$$

where $\Delta r = c\tau/2$, t_i is the sample time of the ith pair's first sample, and the superscript (*) represents a complex conjugate. Since the cross-polarized signals are scattered from cells located at ranges $r \pm \Delta r$, only $V_{hh}(r)$ and $V_{vv}(r)$ are correlated, and therefore the expectation ($\langle\ \rangle$) of the estimated cross-correlation function reduces to

$$\langle\hat{R}_{vh}(r,\tau)\rangle = \langle V_{vv}(r,t)V_{hh}(r,t+\tau)^*\rangle. \quad (14)$$

For h–v pairs, the expression for $\langle\hat{R}_{hv}(r,\tau)\rangle$ takes a similar form except that the v's and h's are interchanged in (14).

Cross-polarization interference, phase noise, and thermal noise do not bias the phase of $\langle\hat{R}\rangle$ and therefore do not bias the estimated mean velocity; however, they do increase the standard deviation of the velocity estimate. From (13) it can be shown (see the appendix) that, if the number of independent pulse-pair samples M is sufficiently large, the variance of the unbiased mean velocity estimate, $\sigma^2_{\hat{\mu}_u}$, can be approximated as

$$\sigma^2_{\hat{\mu}_u}(r) = \frac{u^2_{\max}}{2M[\pi|R_{vh}(r,\tau)|]^2}[P^2_{co}(r) - |R_{vh}(r,\tau)|^2 + P_{co}(r)P_{cross}(r+\Delta r) + 2P_{co}(r)P_n + P_{cross}(r-\Delta r)P_{co}(r) + P_{cross}(r-\Delta r)P_{cross}(r+\Delta r) + P_{cross}(r-\Delta r)P_n + P_nP_{cross}(r+\Delta r) + P^2_n], \quad (15)$$

where $P_{co}(r) = \langle|V_{vv}(r)|^2\rangle = \langle|V_{hh}(r)|^2\rangle$, $P_{cross}(r) = \langle|V_{vh}(r)|^2\rangle = \langle|V_{hv}(r)|^2\rangle$, $P_n = \langle|N_v|^2\rangle = \langle|N_h|^2\rangle$, and M represents $M/2$ independent v–h pairs combined with $M/2$ independent h–v pairs. To simplify (15), the following assumptions have been made: no differential reflectivity, reciprocity ($S_{vh} = S_{hv}$) (Zrnić 1991), and equal gain in the two orthogonally polarized channels of the radar.

To evaluate σ_{μ_u}, the power terms P_{co} and P_{cross} can be measured directly, or (11) can be evaluated if $\mathbf{D}_T$, $\mathbf{D}_R$, $\mathbf{S}$, and $\mathbf{D}_P$ are known or can be approximated; matrices $\mathbf{D}_T$ and $\mathbf{D}_R$ can be obtained as a result of a polarimetric calibration of the radar (Wood 1986) and $\mathbf{S}$; and $\mathbf{D}_P$ can be approximated based on the shape and composition of the particles that are located in the radar beam. Note that, if P_{cross} is zero and the cross-correlation function R_{vh} is replaced by the autocorrelation function R, (15) reduces to the expression for the variance of conventional pulse-pair mean velocity estimate, which is given by Doviak and Zrnić (1984) as

$$\sigma^2_{\hat{\mu}_u} = \frac{u^2_{\max}}{2\pi^2\beta^2M}[(1 + \mathrm{SNR}^{-1})^2 - \beta^2], \quad (16)$$

where SNR is the signal-to-noise ratio.

Figure 2 presents a comparison between PDPP and conventional pulse-pair estimate standard deviation as a function of range and spectral width using (15) and (16). The following conditions were assumed for these calculations:

- 3-mm (95 GHz) radar wavelength,
- uniform scatterer distribution,
- 20-dB signal–to–thermal-noise ratio at a range of 1 km (14 dB at 2 km, 8 dB at 4 km, . . .),
- no attenuation,
- 20-dB polarization isolation between the co- and cross-polarized signals; this isolation includes the effect of radar system isolation and scatterer depolarization,
- conventional pulse-pair spacing of 66 μs ($u_{\max} = \pm 12$ m s^{-1} at 3-mm wavelength),
- PDPP spacing of 10 μs ($u_{\max} = \pm 79$ m s^{-1} at 3-mm wavelength), and
- 100 independent samples used for each estimate.

Figure 2 shows that, for low spectrum width, conventional pulse-pair estimates have lower standard deviation than PDPP estimates, but, as the spectral width

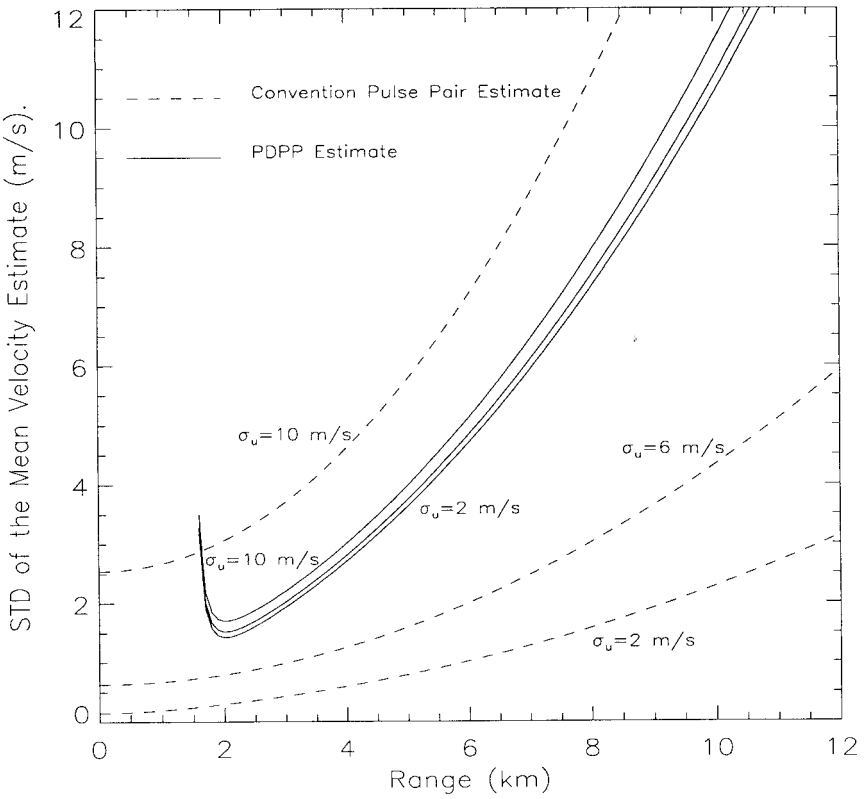

FIG. 2. Comparison of PDPP and conventional pulse-pair mean velocity estimate errors. The errors were calculated for 66 μs ($u_{max} = \pm 12$ m s^{-1} at 95 GHz) conventional pulse pair spacing and 10 μs ($u_{max} = \pm 80$ m s^{-1} at 95 GHz) PDPP spacing, assuming uniform scatterer distribution, 20-dB signal–to–thermal-noise ratio at a range of 1 km, and 20-dB polarization isolation between copolarized cross-polarized signals. The standard deviation of the mean velocity estimates are plotted as a function of range (decreasing signal–to–thermal-noise ratio) for different spectral widths ($\sigma_u = 2$, 6, and 10 m s^{-1}).

increases, conventional pulse-pair estimates degrade and become less accurate than PDPP estimates. This behavior is because when the width of the Doppler spectra approaches the width of the unambiguous velocity range (Nyquist interval), the scattering-process decorrelation time approaches the pulse-pair spacing, and, consequently, the pulses within each pair become less and less correlated. PDPP estimate standard deviation, however, barely is affected by spectral width in the range of 2–10 m s^{-1} because of the high unambiguous velocity. The effect of cross-polarization interference on the PDPP estimate is evident at close range (1.5–2 km), where cross-polarized signal scattered from $r - \Delta r$ interferes with the copolarized signal scattered from r. This interference becomes worse with decreasing r since it is proportional to the square of the ratio of r to $r - \Delta r$.

FIG. 3. The 95-GHz polarimetric cloud radar and chase van during a measurement.

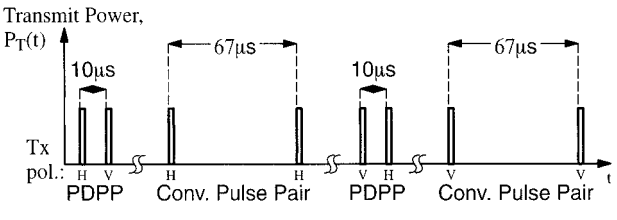

10μs: ±80 ms^{-1} unambiguous Doppler @ 95 GHz.
67μs: ±11 ms^{-1} unambiguous Doppler @ 95 GHz.

FIG. 4. Interleaved PDPP and conventional pulse-pair transmitted pulse sequence.

FIG. 5. Photograph of the wall cloud associated with the southern, cyclonic hook echo. The photo was taken from the radar while the radar image was being recorded. The feature in the center of the photograph is a lightning strike.

An interleaved pulse sequence of PDPP and conventional pulse pairs takes advantage of the benefits of both techniques. Moreover, conventional measurements may be extended several times beyond their maximum unambiguous velocity because, like standard staggered PRF techniques, PDPP measurements can be used to correct folded Doppler data. The next section presents experimental data obtained with such an interleaved pulse sequence.

4. Measurements

Since 1993, the UMass 95-GHz polarimetric cloud radar (Pazmany et al. 1994b, 1994a) has been involved in a joint UMass–OU experiment to study mesocyclones (2–5 km wide in thunderstorms) and tornadoes in the southern plains of the United States (Bluestein et al. 1997, 1995). The 95-GHz radar system, a computer-controlled positioner, and a manual hydraulic lift were installed in an OU van so the radar could be elevated through an opening in the roof to collect data. The radar system also was equipped with a video monitor and camera, which was aligned with the radar beam to help the radar operator scan the radar and record its pointing direction during data collection. Figure 3 illustrates the chase van and the radar as it is deployed during a measurement.

For the 1995 spring tornado season, the radar was configured to interleave both alternating v–h and h–v PDPP pulse pairs and conventional pairs. This pulse sequence, shown in Fig. 4, allowed the radar to map the reflectivity field from 1.5 to 11 km and to measure mean Doppler velocity up to ± 80 m s^{-1} without ambiguity. Data from an observation of a rotating cloud base (Fig. 5) from the Verification of the Origins of Rotation in Tornadoes Experiment (VORTEX) on 17 May 1995 (Bluestein et al. 1997, 1996) illustrates PDPP measurement quality and the ability of a 95-GHz radar to map the reflectivity and Doppler velocity field in a severe storm (Figs. 6–8). The sampled storm had formed south of Tulsa, Oklahoma, and moved northeastward as a supercell (Doswell and Burgess 1993). When the radar crew intercepted the storm, a gust front extended from the southwest to the north, where a wall cloud (Bluestein 1985) had been observed as a lowered cloud base near the edge of the gust front. The gust front was wrapping up cyclonically as it moved by to the north and northeast (Fig. 5).

The radar-observed reflectivity image (not corrected for attenuation) in Fig. 6a shows two mirror-image hook echoes, each 1 km or less in diameter, along the leading edge of the storm. The conventional pulse-pair velocity image in Fig. 6b, although folded, confirms that the southern member of the pair (0.9, 2 km) corresponds to the cyclonically rotating wall cloud that was visible from the van; the northern member (0.1, 2.6 km), not visible from the van, was rotating in an anticyclonic

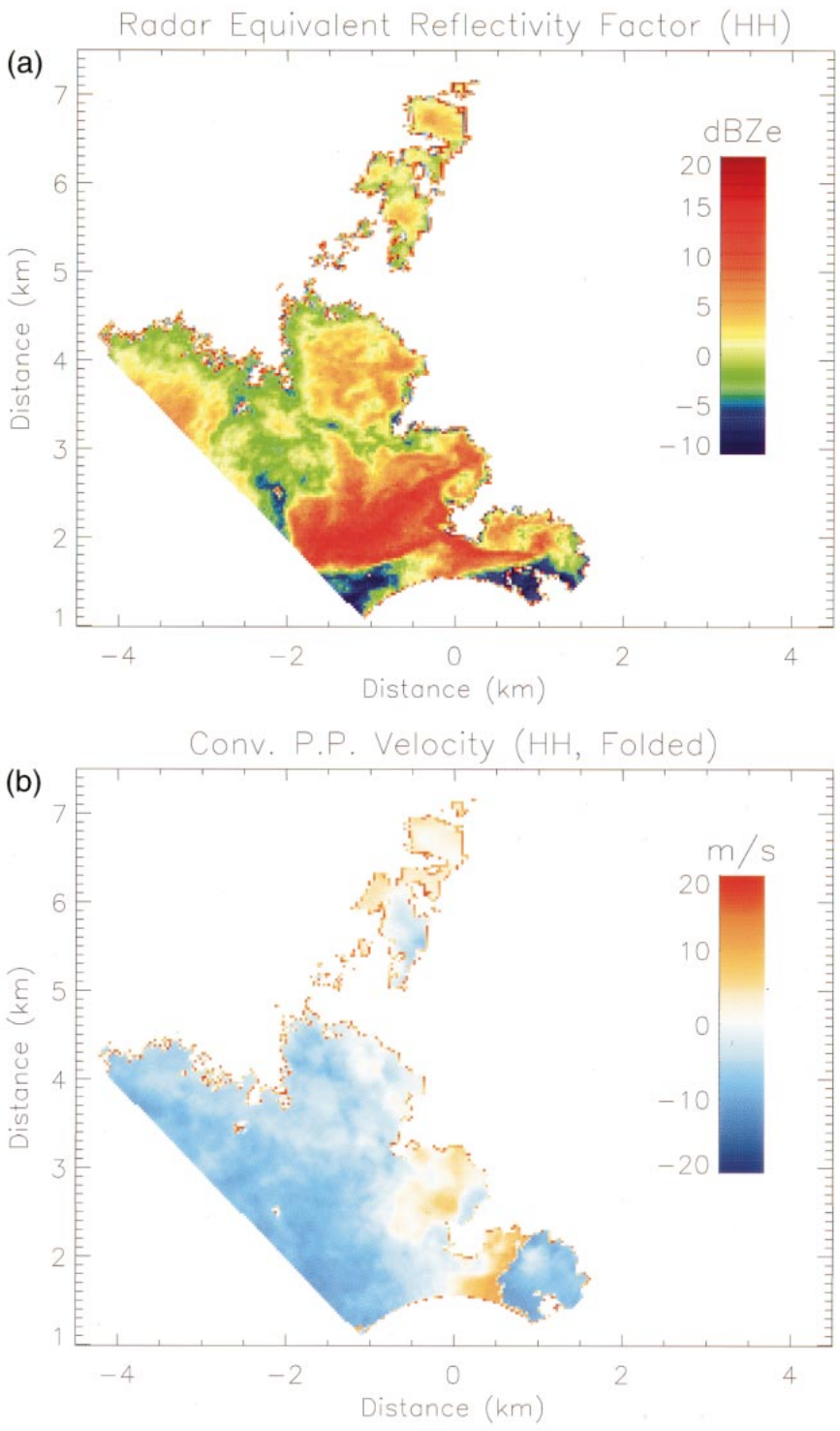

FIG. 6. (a) Radar equivalent reflectivity factor (dBZe) image of the storm feature containing cyclonic and anticyclonic hooks. The image was recorded on 17 May 1995 in northeast Oklahoma, and north is toward the top of the image. (b) Conventional pulse-pair measured velocity image. The measurements are folded where wind speeds exceeded the 11 m s^{-1} maximum unambiguous Doppler velocity. In the velocity images, positive velocities (red colors) indicate motion away from the radar, and negative velocities (blue colors) indicate motion toward it.

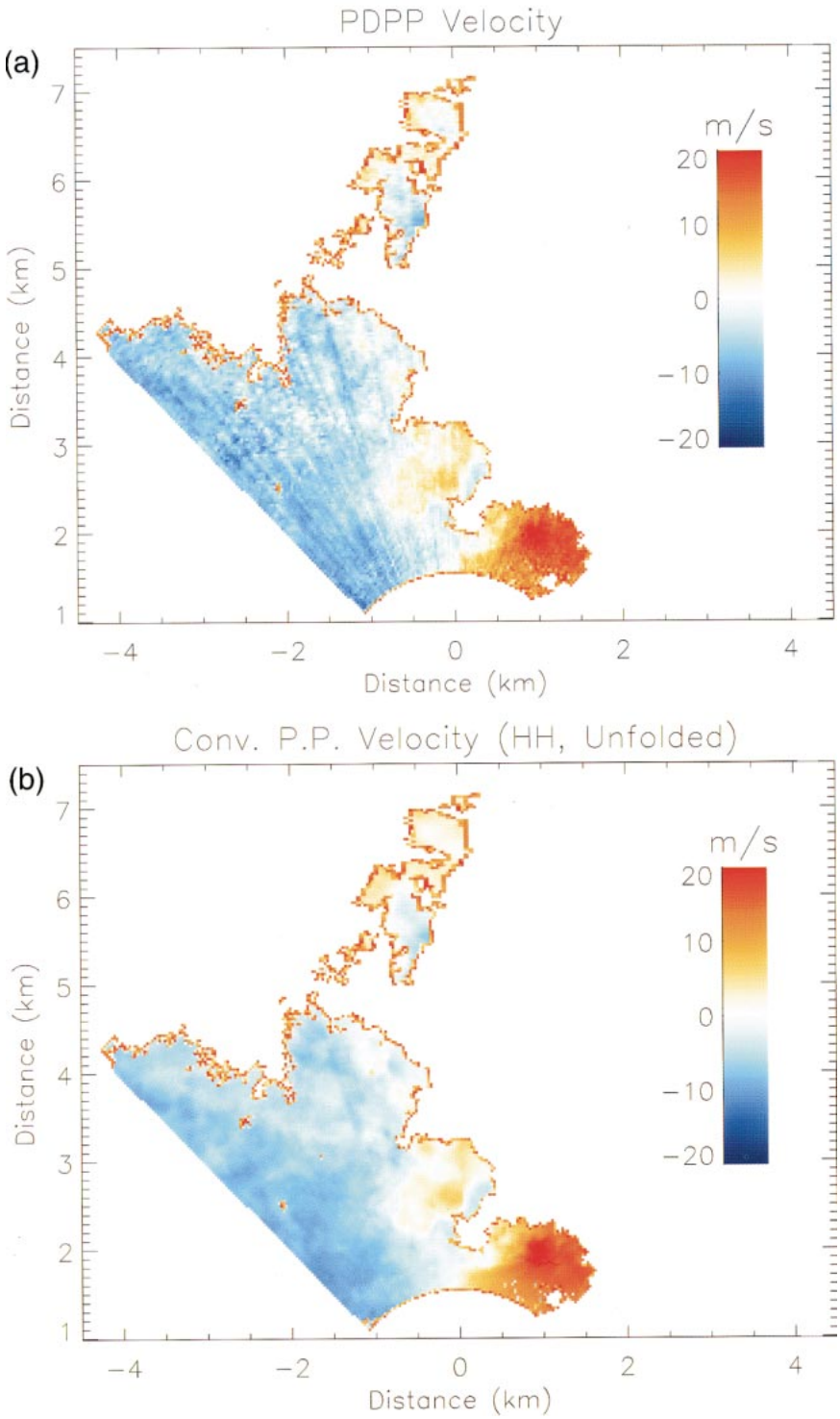

FIG. 7. (a) Polarization diversity pulse-pair velocity image. The ± 20 m s^{-1} velocity range was sufficient to display the wind field, although the data were recorded at ± 80 m s^{-1} maximum unambiguous velocity. (b) Unfolded conventional pulse-pair velocity image.

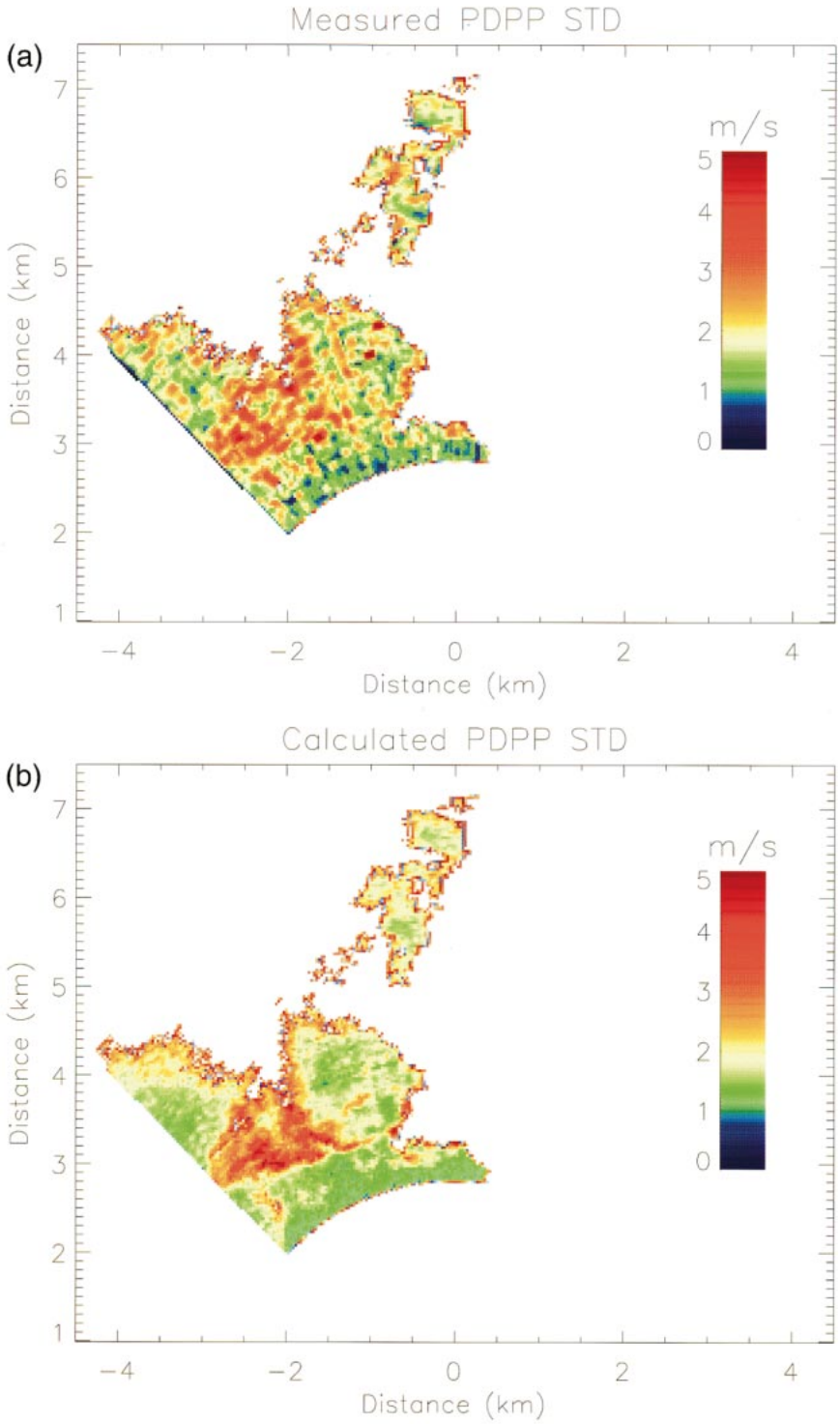

FIG. 8. (a) Measured standard deviation of the PDPP velocity estimate of Fig. 7a. The white arc at 3-km range indicates the minimum range of the calculated standard deviation image in Fig. 11. (b) Calculated [using (15)] standard deviation of the PDPP velocity estimate of Fig. 7a.

direction. The hook echoes apparently were associated with counterrotating vortices.

The corresponding PDPP Doppler velocity image in Fig. 7a, depicts a similar windfield with inferior precision but better accuracy in regions where conventional pulse pairs folded in Fig. 6b. The PDPP measurements were sufficiently precise, however, to locate these folded regions and to reveal the number of folds (wind speeds did not exceed 33 m s^{-1} so double- or higher-order folding did not occur in this dataset). The unfolded conventional pulse-pair image is shown in Fig. 7b. Since the storm feature did not contain regions with high spectral width, such as those associated with a tornado, the conventional pulse-pair measurements were more precise everywhere in the image than were the PDPP measurements.

To test the validity of (15), σ_{μ_u} was calculated for each point in the storm feature image using (15) and was compared to the standard deviation in the PDPP velocity image. Since the data acquisition system recorded only the radar parameters from 1.5 to 9 km, σ_{μ_u} could be calculated only from 3 to 7.5 km [(15) requires $P_{\text{cross}}(r \pm \Delta r)$]. The standard deviation of the radar-measured Doppler velocity was estimated spatially from Fig. 7a using a 3 × 3 pixel window (about 90 m × 90 m area at a range of 3 km). The window was centered on each point in the PDPP image and the standard deviation of the enclosed nine points was calculated. The same procedure then was implemented on the conventional pulse-pair image to estimate and to correct for the spatial variation in the actual wind field over the 3 × 3 pixel window. The resulting image of this ''measured'' standard deviation is shown in Fig. 8a, and, although noisier, in magnitude it agrees well with the calculated σ_{μ_u}, shown in Fig. 8b.

5. Conclusions

The data presented in this paper demonstrate the feasibility and the benefit of PDPP technique and how PDPP enables millimeter-wave radars to be used to image severe storm dynamics, including tornadoes and hurricane-force winds. The implementation of the PDPP technique requires a radar system with two orthogonally polarized transmitters and receivers, the capability to switch the transmit polarization rapidly from pulse to pulse, and the capability to receive simultaneously the scattered field from both pulses. High polarization isolation between the two channels is necessary to minimize measurement errors.

The benefit of the PDPP technique is the ability to measure Doppler velocity from long range up to extreme speeds even when the standard deviation of the Doppler spectrum is large; its weakness is the lack of accuracy compared to that of conventional pulse pairs in moderate to low wind conditions and at short ranges. To take advantage of the benefits of both techniques, PDPP may be interleaved with conventional pulse pairs. This pulse sequence may be the ideal ''staggered'' PRF because it can be effective in almost any weather condition and measurement configuration.

Acknowledgments. The authors wish to thank Bruce Williams for preparing the radar for the experiment, and David Dowell, Herb Stein, Todd Crawford, and Todd Hutchinson for their help during the storm chases. This work was supported by NSF Grant ATM-9616730 and a supplement to NSF Grant ATM-9320672 at UMass and by supplements to NSF Grants ATM-9019821 and ATM-9302379 at OU.

APPENDIX

Standard Deviation of the Polarization Diversity Pulse Pair Estimate of the Mean Velocity

The estimate of the cross-correlation function $\hat{R}_{vh}$ from (13) corresponding to range and pulse spacing can be expressed in terms of copolarization, cross-polarization and thermal noise voltages at the output of a radar receiver as

$$\hat{R}_{vh}(r,\tau) = \frac{1}{M}\sum_{i=1}^{M}\{[V_{vv}(r,t_i) + V_{vh}(r-\Delta r,t_i) + N_v(t_i)] \times [V_{hh}(r,t_i+\tau) + V_{hv}(r+\Delta r,t_i+\tau) + N_h(t_i+\tau)]^*\}, \quad \text{(A1)}$$

where M is the number of independent pulse-pair samples, r is range, the subscripts vh of $R_{vh}(r)$ denote vertical–horizontal pulse pairs, τ is the pulse spacing within the pairs, $\Delta r = c\tau/2$, V_{ij} is the received voltage at i polarization when j polarization was transmitted, and N_i is thermal noise voltage in the i-polarized receiver. Since only V_{vv} and V_{hh} are correlated in (A1), the expected value ($\langle\rangle$) of $\hat{R}_{vh}$ reduces to the cross-correlation function R_{vh}:

$$R_{vh}(r) = \langle\hat{R}_{vh}(r)\rangle = \langle V_{vv}(r,t)V_{hh}^*(r,t+\tau)\rangle. \quad \text{(A2)}$$

The estimated cross-correlation function can be separated into R_{vh} and, $\tilde{R}_{vh}$, a complex, random component with uniformly distributed phase (see Fig. A1). The variance of the magnitude of this random component $\sigma^2_{|\tilde{R}_{vh}|}$ can be expressed as

$$\sigma^2_{|\tilde{R}_{vh}(r)|} = \frac{1}{M}[P_{vv}(r)P_{hh}(r) - |R_{vh}(r)|^2 + P_{vv}(r)P_{hv}(r+\Delta r) + P_{vv}(r)P_{nh} + P_{vh}(r-\Delta r)P_{hh}(r) + P_{vh}(r-\Delta r)P_{nh} + P_{vh}(r-\Delta r)P_{hv}(r+\Delta r) + P_{nv}P_{hh}(r) + P_{nv}P_{hv}(r+\Delta r) + P_{nv}P_{nh}], \quad \text{(A3)}$$

where P_{ij} is the average power at the output of the i-polarized receiver when j polarization was transmitted, and P_{nv} and P_{nh} are the average noise power in the vertical and horizontal receivers, respectively.

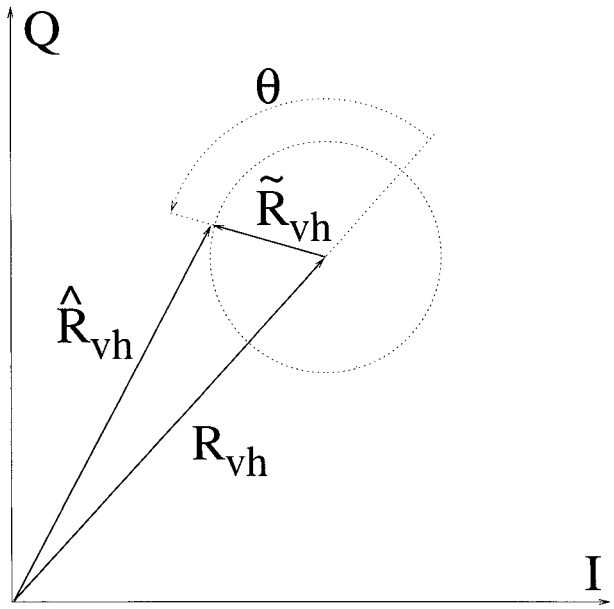

FIG. A1. Decomposition of the measured complex cross relation $\hat{R}_{vh}$ into the actual cross correlation R_{vh} and a random component $\tilde{R}_{vh}$.

The phase ϕ of $\hat{R}_{vh}$ can be expressed as

$$\phi = \arctan\left(\frac{|\tilde{R}_{vh}|\sin(\theta)}{|R_{vh}|}\right) + \arg[R_{vh}], \quad \text{(A4)}$$

where θ is the difference between the phase of $\tilde{R}_{vh}$ and the phase of R_{vh}, and is a uniformly distributed random variable from $-\pi$ to π. If sufficient numbers of independent pairs are averaged so $\langle|\tilde{R}_{vh}|\rangle \ll |R_{vh}|$, (A4) simplifies to

$$\phi = \frac{|\tilde{R}_{vh}|\sin(\theta)}{|R_{vh}|} + \arg[R_{vh}], \quad \text{(A5)}$$

and, since θ is distributed uniformly and is independent of $|\tilde{R}_{vh}|$ and $|R_{vh}|$, the expectation of the measurement phase reduces to

$$\langle\phi\rangle = \arg[R_{vh}]. \quad \text{(A6)}$$

The variance of the measured phase σ_ϕ^2 can be related to the cross-correlation function by evaluating the integral

$$\sigma_\phi^2 = \frac{1}{|R_{vh}|^2}\int_0^\infty x^2 f_{|\tilde{R}_{vh}(r)|}(x)\,dx \int_{-\pi}^{\pi}\frac{1}{2\pi}\sin^2(\theta)\,d\theta, \quad \text{(A7)}$$

where $f_{|\tilde{R}_{vh}(r)|}$ is the distribution function of $|\tilde{R}_{vh}|$. The resulting expression for the variance of the measurement phase is

$$\sigma_\phi^2 = \frac{\sigma^2_{|\tilde{R}_{vh}(r)|}}{2|R_{vh}|^2}. \quad \text{(A8)}$$

Since Doppler velocity u is related to the measurement phase according to

$$u = \phi\lambda/4\pi\tau, \quad \text{(A9)}$$

the standard deviation of the velocity estimate $\sigma_{\hat{\mu}_{vh}}$ can be expressed as

$$\sigma_{\hat{\mu}_{vh}} = \frac{\lambda}{4\pi\tau}\sqrt{\frac{\sigma^2_{|\tilde{R}_{vh}(r)|}}{2|R_{vh}(r)|^2}}. \quad \text{(A10)}$$

Similarly, the standard deviation of the velocity estimate from h–v pairs $\sigma_{\hat{\mu}_{hv}}$ is

$$\sigma_{\hat{\mu}_{hv}} = \frac{\lambda}{4\pi\tau}\sqrt{\frac{\sigma^2_{|\tilde{R}_{hv}(r)|}}{2|R_{hv}(r)|^2}}, \quad \text{(A11)}$$

where

$$\begin{aligned}\sigma^2_{|\tilde{R}_{hv}(r)|} = \frac{1}{M}[&P_{hh}(r)P_{vv}(r) - |R_{hv}(r)|^2 + P_{hh}(r)P_{vh}(r+\Delta r)\\ &+ P_{hh}(r)P_{nv} + P_{hv}(r-\Delta r)P_{vv}(r)\\ &+ P_{hh}(r-\Delta r)P_{nv} + P_{hv}(r-\Delta r)P_{vh}(r+\Delta r)\\ &+ P_{nh}P_{vv}(r) + P_{nh}P_{vh}(r+\Delta r) + P_{nh}P_{nv}].\end{aligned} \quad \text{(A12)}$$

Since the unbiased velocity estimate is obtained from the average of v–h and h–v pulse-pair phase measurements, the standard deviation of the unbiased velocity estimate, $\sigma_{\hat{\mu}_u}$, is

$$\sigma_{\hat{\mu}_u} = 1/2(\sigma^2_{\hat{\mu}_{vh}} + \sigma^2_{\hat{\mu}_{hv}})^{1/2}. \quad \text{(A13)}$$

REFERENCES

Bluestein, H. B., 1985: Wall clouds with eyes. *Mon. Wea. Rev.*, **113,** 1081–1085.

——, A. L. Pazmany, J. C. Galloway, and R. E. McIntosh, 1995: Studies of the substructure of severe convective storms using a mobile 3-mm-wavelength Doppler radar. *Bull. Amer. Meteor. Soc.*, **76,** 2155–2169.

——, ——, D. C. Dowell, J. C. Galloway, R. E. McIntosh, H. Stein, and S. Gaddy, 1996: Observations of sub-storm scale vortices in supercells using a mobile, 3-mm wavelength, pulsed Doppler radar. Preprints, *18th Conf. on Severe Local Storms Conf.*, San Francisco, CA, Amer. Meteor. Soc., 23–26.

——, S. G. Gaddy, D. C. Dowell, A. L. Pazmany, J. C. Galloway, and R. E. McIntosh, 1997: Doppler radar observations of sub-storm-scale vortices in a supercell. *Mon. Wea. Rev.* **125,** 1046–1059.

Doswell, C. A., and D. W. Burgess, 1993: Tornadoes and tornadic storms: A review of conceptual models. *The Tornado: Its Structure, Dynamics, Prediction, and Hazards, Geophys. Monogr.*, No. 79, Amer. Geophys. Union, 161–172.

Doviak, R. J., and D. Sirmans, 1973: Doppler radar with polarization diversity. *J. Atmos. Sci.*, **30,** 737–738.

——, and D. S. Zrnić, 1984: *Doppler Radar and Weather Observations.* Academic Press, 458 pp.

Golestani, Y., V. Chanderasekar, and R. J. Keeler, 1995: Dual polarization staggered PRT scheme for weather radars: Analysis and application. *IEEE Trans. Geosci. Remote Sens.*, **33,** 239–246.

Mead, J. B., P. S. Chang, S. P. Lohmeier, P. M. Langlois, and R. E. McIntosh, 1993: Polarimetric observations and theory of millimeter-wave backscatter from snow cover. *IEEE Trans. Antennas Propag.*, **41,** 38–46.

Miller, K. S., and M. M. Rochwarger, 1972: A covariance approach to spectral moment estimation. *IEEE Trans. Inf. Theory*, **18,** 588–597.

Pazmany, A. L., and R. E. McIntosh, 1994: The use of estimation

techniques to reduce noncoherent polarimetric measurement errors. *IEEE Trans. Antennas Propag.,* **42,** 1325–1328.

——, ——, R. D. Kelly, and G. Vali, 1994a: An airborne 95 GHz dual-polarized radar for cloud studies. *IEEE Trans. Geosci. Remote Sens.,* **32,** 731–739.

——, J. B. Mead, R. E. McIntosh, M. Hervig, R. Kelly, and G. Vali, 1994b: 95-GHz polarimetric radar measurements of orographic cap clouds. *J. Atmos. Oceanic Technol.,* **11,** 140–153.

Wood, A. M., 1986: A theoretical study of calibration procedures for coherent and noncoherent polarimetric radars. Tech. Rep. 86011, Royal Signals and Radar Establishment, Malverne, 43 pp.

Zrnić, D. S., 1997: Spectral moment estimates from correlated pulse pairs. *IEEE Trans. Aerosp. Electron. Syst.,* **13,** 344–345.

——, 1991: Complete polarimetric and Doppler measurements with a single receiver radar. *J. Atmos. Oceanic Technol.,* **8,** 159–165.